ELSEVIER

Deep-Sea Research II 51 (2004) 551–561

DEEP-SEA RESEARCH
PART II

www.elsevier.com/locate/dsr2

Ekman modulation of the sea-surface temperature on the Eastern South Pacific

Luis Soto-Mardones[a,b,*], Alejandro Parés-Sierra[c], Reginaldo Durazo[b]

[a] *Universidad del Bio-Bio, Concepción–Chile*
[b] *Universidad Autónoma de Baja California, Ensenada–México*
[c] *Centro de Investigación Científica y de Educación Superior de Ensenada, Ensenada–México*

Received 15 October 2002; accepted 3 May 2004

Abstract

Nine years of data (1992–2000) were used to study the evolution of the sea–surface temperature (SST) over the eastern south Pacific. Our analysis shows that the variability in the SST on the interannual scale is attributed mainly to the equatorial El Niño-La Niña events while cooling, associated with the wind-Ekman drift, is an important component of the annual cycle.

The anomalies at the interannual scale show up as a front that parallels the coast. At the seasonal scale, anomalous warming and cooling of coastal waters is strongly altered by the local effect of the wind-driven Ekman transport. This latter effect is especially significant along the Peruvian and Northern Chilean coast where wind induced upwelling and cooling is out-of-phase with other important annual forcings (i.e radiation and annual Kelvin waves). These local wind effects show up in the time-latitude plots as a thinning of the warm-water bands along the Peruvian coast (~10°S y 17°S) and a thickening of the bands further south (~18°S y 22°S).

Three anomalous events that stand out clearly at the interannual scale are El Niño 92–93, La Niña 96 and El Niño 97–98. Their individual evolutions over time and along the coast are very different. Though the least intense of the three, the 92–93 event had the longest duration. The 96 event was the shortest in duration and its strongest anomaly occurred around the Peruvian coast, similar to the warm event of 92–93. The strongest event for the period occurred in 97–98, its warm anomaly showing strongly along the whole latitudinal extent of the study area.

Contrary to what occurs at the seasonal scale, the increase on east/west Ekman transport on the interannual scale seems to be in phase with other relevant cooling and warming mechanisms. The interannual Ekman anomalous transports are at their maximum near the Peruvian-northern Chilean coast; however, they do not seem to alter the SST in a significant way. A similar situation has been described for sea-level data in the California Current System, i.e. interannual variability being associated mostly with variability of equatorial origin while seasonal variability is associated to both wind-forced local variability and remotely forced variability (J. Geophys. Res. 94 (1989) 3159)

*Corresponding author. Universidad del Bio-Bio, Concepción–Chile.
E-mail address: lsoto@cicese.mx (L. Soto-Mardones).

0967-0645/$ - see front matter © 2004 Elsevier Ltd. All rights reserved.
doi:10.1016/j.dsr2.2003.06.006

1. Introduction

Sea-surface temperature (SST) variability near the coast is modulated by solar radiation and by local variations in the wind stress. The coastal region between the equator and 40°S on the eastern Pacific is especially interesting since variability also can be strongly altered by the passage of local and remotely forced coastal trapped waves.

Over the eastern south Pacific Ocean, coastal upwelling occurs almost throughout the year, though it is more intense during spring and summer (Pizarro et al., 1994; Huyer et al., 1987; Pizarro, 1999; Soto-Mardones et al., 2004). Large-scale winds over the area are controlled by the counter-clockwise high-pressure cell of the tropical South Pacific. On the northern limit, high precipitation rates along with weak and variable winds are observed at the inter-tropical convergence zone. The northern branch of the high-pressure center (the wind train) drives easterly and southeasterly winds, while the southern branch consists of very intense westerlies. Between 5°S and 35°S, the wind stress has an important alongshore component which favors upwelling throughout most of the year.

The annual variability of wind stress is related to the northern extension of westerly winds. During the southern summer, westerly winds dominate south of 37°S. During winter, these are displaced as far north as 30°S. Nearshore, westerly winds weaken rapidly into two branches and produce a transition zone. This region separates the Chilean coast from two different wind regimes. Towards the north, upwelling favorable winds prevail while downwelling favorable winds are usually observed to the south (Pizarro, 1999). Wind stress is greatest along the Peruvian coast during the southern winter, while the strongest upwelling favorable winds occur during spring around 30°S along central Chile.

On the annual and interannual scales, locally and remotely (equatorial) forced coastally trapped waves propagate towards the south. These are responsible for most of the variability of coastal currents, sea-level and mass fields (Shaffer et al., 1997; Pizarro, 1999; Hormazabal et al., 2001).

In this work, we examine the annual and interannual SST variability along the eastern South Pacific coast, from the equator south to 40°S We do this based on Advanced Very High Resolution Radiometer (AVHRR) satellite images and satellite-derived winds.

2. Data and methods

The wind-stress data incorporated herein were measured by scatterometers onboard the ERS1 and ERS2 satellites at a spatial resolution of $1^\circ \times 1^\circ$. Data sets for the period of September 1991 to October 1999 were obtained from the Département d'Oceanographie Spatiale, IFREMER, France (www.ifremer.fr/droos). Data processing and validation techniques followed instructions detailed in the Scientific User Manual included on CDs (see Shaffer et al., 1999 and Hormazabal et al., 2001 for methodology). Meridional and zonal wind stress were used to construct time series of alongshore wind stress, which were then used to compute Ekman transport.

The new generation of NOAA6 and NOAA polar orbit satellites are equipped with AVHRR sensors. They have 4 or 5 channels, one of which is in the visible range of 1.1 μm. Their instantaneous visual field has a terrestrial resolution of approximately 1.1 km at the nadir. The main sources of error inherent in SST data obtained from radiometers are the absorption of infrared radiation by water vapor present in the atmosphere and the presence of small clouds inside the visual field of sensors. Bernstein (1982) compared SST obtained by AVHRR sensors to that taken from ships and buoys. He correlated these measurements and concluded that remote and in situ data were identical within levels of error less than 0.5 °C.

AVHRR SST data used in this study are part of the global analyses of SST done routinely by the University of Miami, Rosentiel School of Marine and Atmospheric Sciences. Files are global weekly averages with a resolution of 9×9 km. Areas where the presence of clouds hindered the measurement of radiance were filled using both time and spatial interpolation (Case and Cornillon, 1999). Land values were flagged and

the geographical position assigned to each mesh element were related to the central point.

3. Results

3.1. Alongshore wind stress time series

Fig. 1 shows the latitudinal variation of the monthly wind stress along the coast (1A), its standard deviation (1B) and a map of the coastline (1C). The along-shore wind stress is essentially positive (i.e. equatorward) for most of the study area throughout most of the year (Fig. 1A). Only at the southernmost region, south of 35°S, are there certain months during the austral winters (Pizarro, 1999) when winds flow poleward. Accordingly, this indicates upwelling-favorable wind during the majority of the year for the whole region. The strength of the wind variability around the mean changes with latitude (Fig. 1B). It is weaker along the equatorial band (0 – 5°S) and between 15°S and 25°S and is strongest south of 25°S. There is a relative maximum along the Peruvian coast between 10°S and 15°S.

Off Peru, the seasonal maximum of upwelling-favorable winds occur during fall, winter and spring. Bakun and Nelson (1991) had reported this same occurance of upwelling-propitious winds, but only during fall and winter. The seasonal strong winds were further strengthened during El Niño of 1992 and the initial phase of El Niño 1997. During this period, there was an increase in the latitudinal component of the area of wind reversal that occurs normally in winter in the southernmost region. On the average this area reaches approximately 37°S (Pizarro, 1999). However, in the winter of 1996 it reached up to 28°S. There is a conspicuous transition zone of very weak stresses between 16°S and 20°S.

The strongest upwelling favorable winds occur south of approximately 20°S and north of 37°S. They are associated with the South Pacific high. These winds intensify and their relative maximum ($\sim 6 \times 10^{-2}$ Nm^{-2}) shifts southward during the southern spring and summer, as reported by Schwerdtfeger (1976). The low pressure center over land and the system of highs offshore both drive alongshore equatorward winds to create maximum stresses during spring and summer. The relative maximums do not occur simultaneously in Peru and Chile, as noted by several authors (eg. Montecinos, 1991; Fuenzalida, 1992; Carvajal, 1994; Pizarro et al., 1994). Downwelling favorable wind events intensify in winter during the interannual events (1992, 1996 and 1997).

Over the southernmost region, upon reaching the South American coast, westerly winds alternate between the strong northerly winds (associated with the latitudinal displacement of polar fronts during winter) and the southerly winds driven by the subtropical anticyclonic high (which intensify during summer). The seasonal wind stress between 35°S and 40°S is similar to that found in the northeast Pacific between 35°N and 50°N. Across these latitudes, synoptic perturbations of polar fronts drive downwelling favorable winds throughout the year. These winds and the high precipitation rates observed in southern Chile are analogous to processes observed in British Columbia and Alaska in the northern hemisphere (Strub et al., 1998).

3.2. Latitudinal SST time series

The time series of SST along the coast (~30 km offshore, i.e. 3 pixels) versus latitude are shown in color in Fig. 2. Figure 2 also shows contours of temperature advected from the bottom of the Ekman layer (we leave the discussion of these latter contours for Section 3.3). SST has a strong seasonal signal. Higher SSTs are found over the equatorial band (0 – 5°S) and diminish to the south. Wider (longer duration) warm bands occurring during the southern summer are associated with El Niño (eg. 1992–93, 1997–98). Thinner (shorter duration) bands are associated to La Niña (eg. 1996). As is evident in this figure, an important feature of the SST is the anomalous thinning of the summer warm bands off the coast of Peru, approximately between 10°S and 16°S. Over this latitudinal range, the lowest SSTs are recorded during the winter in concordance with the intense upwelling events of the season, as noted by Weare et al. (1980) and Halpern et al. (1992). Between 16°S and 20°S, these bands again thicken

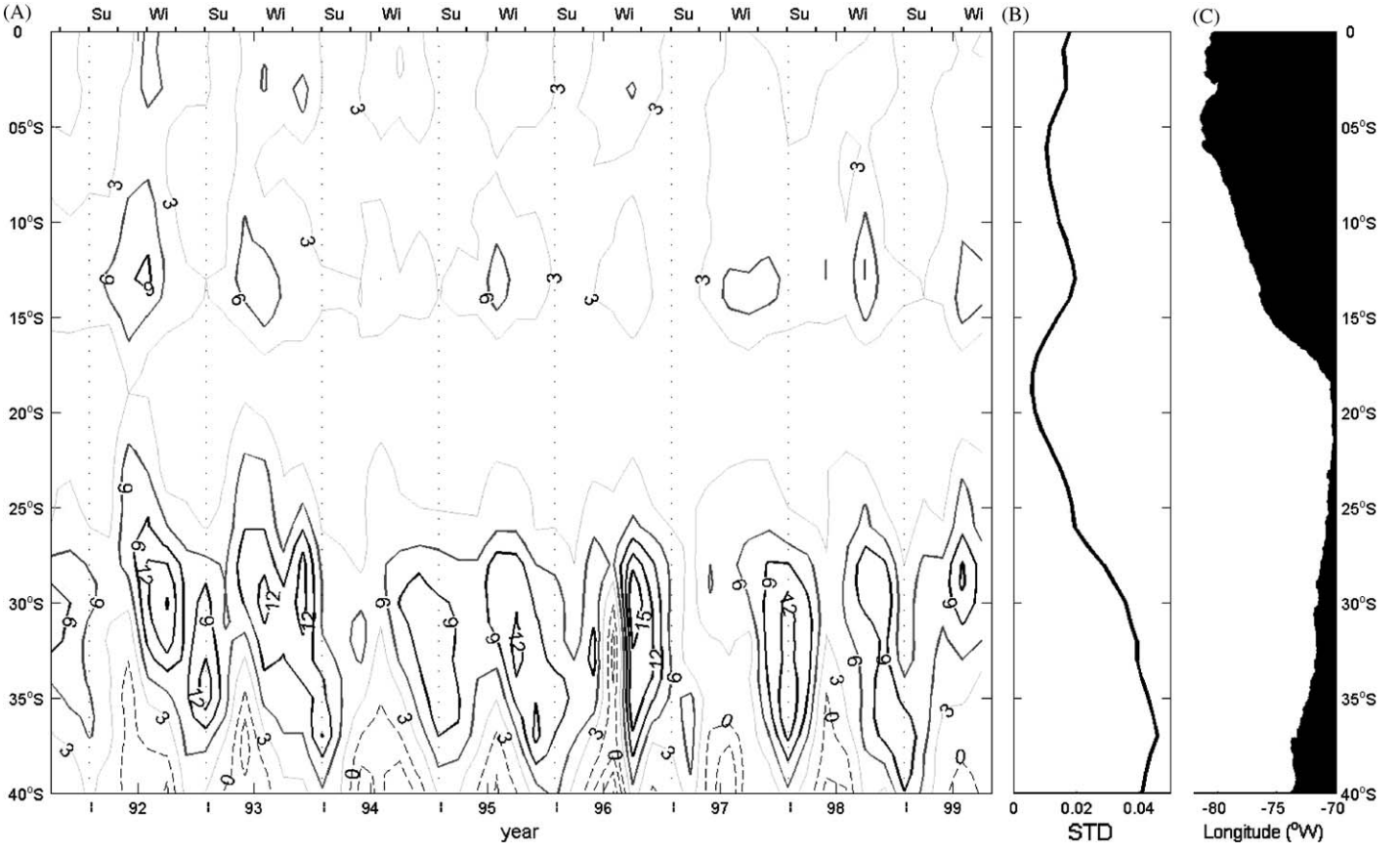

Fig. 1. (A) Temporal distribution of wind stress ($10^{-2}\,N\,m^{-2}$) parallel to coast, from September 1991 to October 1999 (solid lines indicate winds to the north), (B) its standard deviation and (C) the coast of South America.

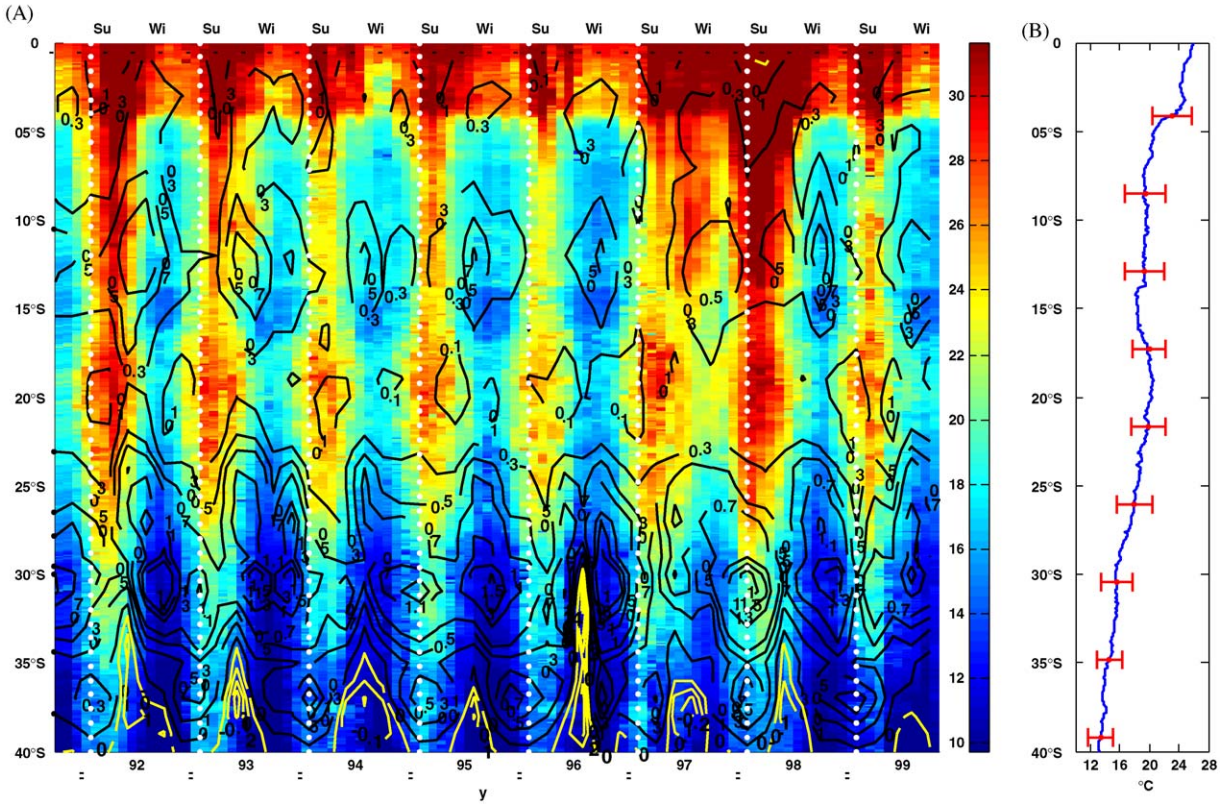

Fig. 2. (A) Annual variability of SST along the coast (color) and surface cooling (°C month^{-1}) due to Ekman advection (black contours). (B) Long-term mean of the SST along the coast.

with even higher temperatures associated with a latitudinal relative minimum in wind stress (Fig. 1A) and with the change of orientation of the coastline from Peru to Chile (Fig. 1B). Although seemingly of less amplitude, the seasonal cycle of SST is still evident south of these latitudes. As will be shown in next section, this somewhat strange behavior of showing a smaller seasonal cycle at high latitudes is due to the anomalous cooling of Ekman drift.

The mean latitudinal variation of SST and its standard deviation are depicted in Fig. 2B. While mean temperature is at a minimum in southern latitudes and at a maximum toward the equatorial region, an interesting relative minimum is observed off the coast of Peru between 5°S and 16°S. The latitudinal variability of standard deviation follows that of SST, as variability is at a minimum in southern latitudes.

In order to discriminate between the mechanisms that control SST, we isolated the seasonal component, which is arguably the largest contribution to the signal. The mean SST (Fig. 2B) and the interannual signal (shown later in Fig. 5) were subtracted from the monthly SST field (Fig. 2A). SST anomalies associated with the annual signal are shown in Fig. 3A. Alternating warming and cooling bands are more clearly defined in this figure. The core of the warm bands have a south-to-north positive inclination (~3 months) in accordance with the geometry of the solar transit during the summer, ie. radiation maximum is first reached on the southern region.

To facilitate the visualization and description of the annual signal, a least squares fit was performed. The data was fitted to

$$\psi(y,t) = \sum \{\phi(y)\exp(i[\omega t - \theta(y)])\}, \quad (1)$$

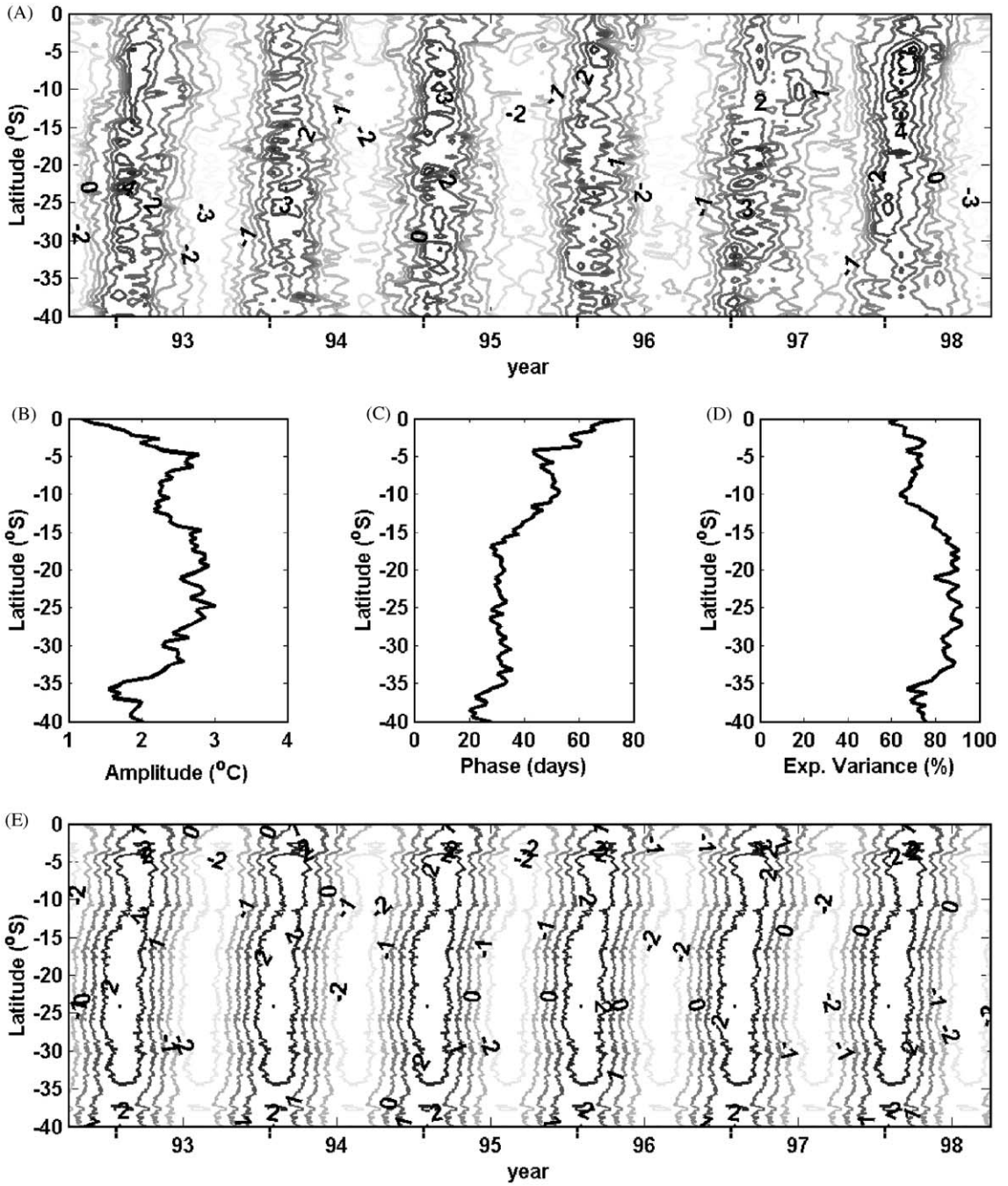

Fig. 3. (A) Latitudinal distribution of SST anomaly time series. The mean and interannual signals have been removed (contour interval is 1 °C). Latitudinal variation of (B) amplitude (°C), (C) phase (days from starting January 1) and (D) percentage of explained variance of the annual component. (E) Annual fit of SST to (A).

where Ψ represents SST, ϕ and θ the amplitude and phase (days from 1 January) of the harmonic with annual frequency ω. The latitudinal variation of amplitude, phase and the percentage of explained variance of SST are shown in Fig. 3B–D, respectively. The largest anomalies are between 5°S and 33°S. A slight decrease, also noted in Fig. 2, is evident in the northern region (5°S – 16°S). The slope of the line in Fig. 3C indicates that maximum warming first occurs in the south and moves northward. It reaches the southern part towards the end of January and affects the region between 15°S and 33°S in early February, as previously noted by Soto-Mardones et al. (2004). Off Peru, maximum warming occurs by mid-February while it transpires near the equator by early March, as noted by Fritz (1951). The variance explained by the annual cycle is approximately uniform along the coast (~80%, Fig. 3D). Fig. 3E depicts the reconstruction of SST in Fig. 3A using the fitted parameters.

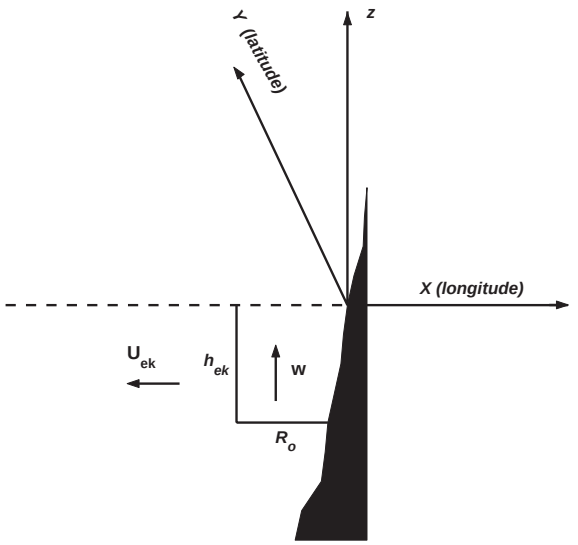

Fig. 4. Schematic diagram showing the continuity balance between Ekman drift velocity (U_{ek}) on the Ekman layer with depth h_{ek} and Ekman pumping w velocity over a Rossby radius of deformation R_o.

3.3. Ekman drift and latitudinal variation of temperature advection

Assuming that the horizontal scaling of upwelling near the coast is the Rossby Radius of deformation (eg. Gill, 1982), a simple balance equation that relates Ekman drift velocity (U_{ek}) to the upwelling velocity (w) from the base of the Ekman, is given by (see Fig. 4)

$$U_{ek}h_{ek} = wR_o, \tag{2}$$

where h_{ek} is the depth of the Ekman layer and R_o is the Rossby radius of deformation so that the rate of change of temperature (T) at the surface due to the advection of upwelling water is

$$\frac{dT}{dt} = \frac{U_{ek}(y,t)h_{ek}(y)}{R_o(y)}\frac{fT(y,t)}{fz}. \tag{3}$$

Here, y is latitude, z is the vertical coordinate and t is time. Ekman drift and Ekman layer depth were computed using the formulas given by Madsen (1977) (see Appendix A).

The vertical gradient of temperature in (3) was estimated using Levitus climatology (Levitus, 1994) for the temperature at the bottom of the Ekman layer and AVHRR for the surface temperature. We assume that most of the non-seasonal variability comes from the surface and that the neglected variability from the depth, implicit in the use of Levitus climatology, is small. By necessity, this is only a rough estimate of the vertical gradient, however we believe it gives the right tendency.

Using alongshore wind stresses (Fig. 1), the rate of change of temperature versus time (°C/month) was computed using Eq (3). The results are depicted as contours in Fig. 2A.

Off Peru, between 8°S and 14°S, large rates of change of temperature are observed year round, with the exception of summer. These high rates carry colder waters from the base of the Ekman layer, cooling the surface and thinning the warm bands at these latitudes. Cross-correlation between SST and dT/dt are shown in Fig. 5. As expected in this area where the effect of cooling by upwelling is significant, these two components are in quadrature (ie. high correlation at approximately half cycle apart, Fig 5). Westward drift velocity reaches its maximum (~10 cm s^{-1}) over this region and drives a strong upwelling of colder water as

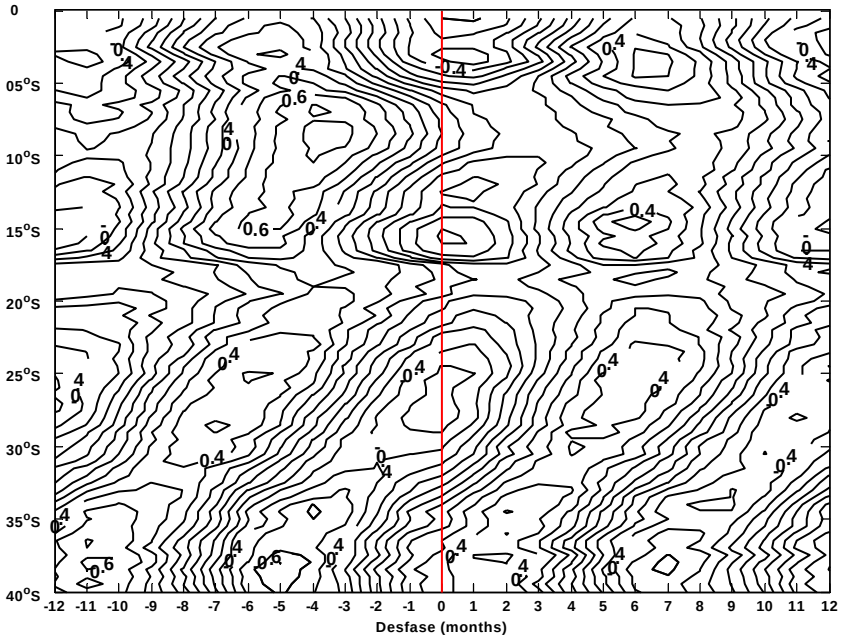

Fig. 5. Cross-correlation between SST and dT/dt. Lags in months.

previously noted by other authors (Rojas de Mendiola, 1981; Richards, 1981; Guillen and Calienes, 1981; Huyer et al., 1987, 1991).

Where the coastline changes direction (16°S–18°S), the contribution of subsurface waters is probably small as the orientation of the coastline hinders meridional winds (Fig. 1A) in the generation of upwelling. Off Chile, between 22°S and 35°S, the rate of change of SST is larger as compared to Peru and is coherent with the maximum wind stress measured there. Although more intense from fall to spring, the rate of change is large throughout the year. Similarly, the westward drift is more intense during spring and summer, as observed previously by Carvajal (1994).

During the southern summer of 1998, in the decaying stage of El Niño 1997–98, the rate of change of SST showed a significant increase. This increase is also observed during El Niño 1992–93. Over the northern region, the same process appearss to occur, but it apparently has no influence on the SST field. Finally, in the southernmost region, between 35°S and 40°S, weak onshore drift velocities are observed as an outcome of westerly winds. The process is then reverted as surface waters sink due to the poleward wind stress.

3.4. Interannual SST time series

SST monthly time series (Fig. 2,) have shown that the width (duration) of warm bands is affected by local nearshore processes. Another process that might influence SST is change due to basin-wide events. SST monthly time series were low-pass filtered to remove the seasonal signal and the result is shown in Fig. 6. SST interannual anomalies clearly show the bands with the decay of El Niño 1992–93 and the mature phase of El Niño 1997–98. Also of note is the cold band associated to La Niña event of 1996. This figure shows how El Niño 1997–98 extends up to the southern end of the domain (40°S) while La Niña is less intense and of limited latitudinal extent. These results agree with what has been discussed for the coasts of Chile (Pizarro et al., 1999; Hormazabal et al., 2001; Blanco et al., 2002).

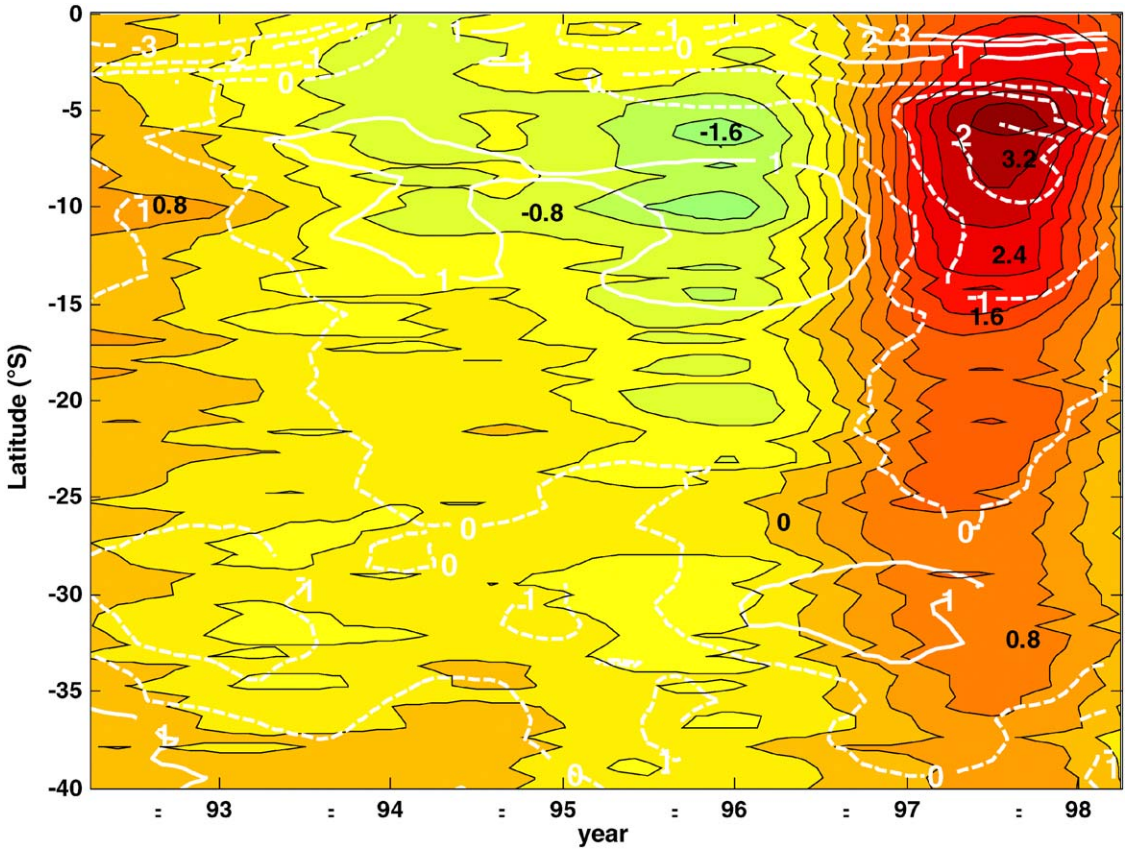

Fig. 6. Latitudinal distribution of the SST interannual anomalies time series °C (color). White contour indicate Ekman drift velocity anomalies (dashed for negative, i.e. westward; continues for positive, i.e. eastward).

4. Discussion and conclusions

SST data and its alongshore temporal rate of change (dT/dt) show clearly that temperature variability nearshore is greatly modulated by the alongshore wind stress. Although the principal forcing on SST is solar radiation, which in turn drives some interannual frequencies (i.e. 1992–93, 1996 and 1997–98), what is striking is the level of coupling shown between observed SST stripes on Fig. 2 and computed contours of SST rate of change.

The orientation of the coastline seems to play an important role on the wind's ability to produce upwelling. Although the maximum wind stresses are located off Chile (Fig. 1), less intense winds off Peru produce surface drift velocities of similar magnitude. The widening of warm bands at the curvature zone between Chile and Peru is likely explained by the weak meridional winds and their unability to produce upwelling and, in turn, modify SST of the surrounding waters. Off Peru (8°S – 16°S), subsurface colder water upwells during fall, winter and spring and produces a decrease in the amount of 0.5 °C/month. Likewise, off Chile (22°S – 35°S), the rate of change in temperature tends to increase even more.

For the interannual scale, Ekman drift velocity anomalies increased to the West during the El Niño period (Fig. 6, white contours). During 1997–98, westward Ekman drift velocity anomalies were very large and located at the SST anomaly maximum. This increase in Ekman drift should inhibit the anomalous warming of SST that occurs at the seasonal scale. However this is not evident from the figure. This is likely because the 97–98

event was so strong that the upwelled water, though at a anomalously large rate, was not cold enough to significantly affect SST; i.e. it did not come from below the layer. In fact, this could also be happening at the seasonal scale, as Ekman drift seems to be less efficient during the 97–98 event (Fig. 2). For La Niña 1996, onshore Ekman drift anomalies were observed in the south. This process carried oceanic waters close to the coast, but they failed to modify the thermal properties of the coastal waters as they originated from similar depths.

From this work, it is possible to conclude that, on the interannual scale, SST is mostly controlled by energy of equatorial origin while, on the seasonal scales, both local (eg. wind-driven Ekman drift) and remote information (e.g., equatorial waves) are important. A similar conclusion was reported for the California Current, another eastern boundary current system, by Pares-Sierra and O'Brien (1989).

Acknowledgements

This work received financial support from CICESE and from Conacyt proyect 225080-5-28799 T. Luis Soto thanks the Organization of American States University of BIO-BIO-CHILE and Universidad Autónoma de Baja California for schorlarship contribution.

Appendix A. The wind-induced Ekman boundary layer

This proposes a physically realistic and general model for the vertical eddy viscosity in a homogeneous fluid. For an infinitely deep ocean the vertical eddy viscosity increases linearly with depth from a value of zero at free surface. Based on this model a general theory is developed for the drift current resulting from a time-varying surface shear stress. Explicit expressions are given for temporal development of the drift current in the vicinity of the free surface and for the steady-state response to a suddenly applied uniform shear stress.

The equation to determine the Ekman layer is:

$$h_{\mathrm{ek}} = k\frac{u_*}{f}. \tag{A.1}$$

As found by Ruggles (1970), by taking $k = 0.4$ and $u_* = 0.04(\frac{\rho_a}{\rho})^{-1/2} W_{10}$ with the ratio of air to fluid density, $\frac{\rho_a}{\rho} = \frac{1}{840}$, Eq. (A1), it is shown that:

$$h_{\mathrm{ek}} \cup 3.66\frac{W_{10}}{\sin(\phi)}, \tag{A.2}$$

where h_{ek} is in meters and wind speed W_{10} (ms^{-1}) measured at 10 m above the still water level. Finally, the Ekman drift is determined by means of the following equations:

$$U_{\mathrm{ek}} = u + \mathrm{iv} = \frac{u_*}{k}\left[\frac{\pi}{2} + \mathrm{i}\left(-1.5 + \ln\left(\frac{30h_{\mathrm{ek}}}{k_{\mathrm{s}}}\right)\right)\right], \tag{A.3}$$

where k_{s} is constant of roughness , with the order of magnitude of $\mathrm{k_s}$ being 5 cm and with h_{ek} given by (A.1).

References

Bakun, A., Nelson, C.S., 1991. The seasonal cycle of wind stress curl in sub-tropical eastern boundary current regions. Journal of Physical Oceanography 21, 1815–1834.

Blanco, J. L., Carr, M. E., Thomas, A. C., Strub, T., 2002. Hydrographic conditions off northern Chile during the 1996–1998 La Niña and El Niño events. Journal of Geophysical Research, 107, 10.1029/2001JC001002.

Carvajal, B., 1994. Transporte y turbulencia y su incidencia en el reclutamiento de la anchoveta (*Engraulis ringers)* en la Zona Norte de Chile (20°S). Biólogo Pesquero Thesis, Universidad Arturo Prat, Iquique, Chile.

Case, K.S., Cornillon, P., 1999. A comparison of satellite and in situ-based sea surface temperature climatologies. Journal Climate 12, 1848–1863.

Fritz, S., 1951. Solar radiant energy and its modification by the earth and its atmosphere. In: Compendium of Meteorology American Meteorology Society Boston, pp. 13–33.

Fuenzalida, R., 1992. Proceso de surgencia en la región norte de Chile, latitudes 20°30′S–21°45′S. Investigaciones Científica y Tecnología. Series Ciencias Marina 2, 79–103.

Gill, A.E., 1982. Atmosphere–ocean dynamics, International Geophysics Series 30, 403.

Guillen, O., Calienes, R., 1981. Upwelling off chimbote. In: Richards, F.A. (Ed.), Coastal Upwelling. American Geophysical Union, Washington DC, pp. 312–326.

Halpern, D., Knauss, W., Brown, O., Wentz, F., 1992. An atlas of monthly mean distributions of SSMI surface wind speed,

Argos bouy drift, AVHRR/2 sea surface temperature, and ECMWF surface wind components during 1989. JPL Publication 92–17. Jet Propulsion Laboratory, Pasadena, CA, 112pp.

Hormazabal, S., Shaffer, G., Letelier, J., Ulloa, O., 2001. Local and remote forcing of sea surface temperature in the coastal upwelling system off Chile. Journal of Geophysical Research 106, 16657–16672.

Huyer, A., Smith, R.L., Paluszkiewicz, T., 1987. Coastal upwelling off Peru during normal and El Niño times. Journal of Geophysical Research 92, 14297–14307.

Huyer, A., Knoll, M., Paluszkiewicz, T., Smith, R.L., 1991. The Peru undercurrent: A study in variability. Deep-Sea Research 38 (Suppl. 1), S247–S271.

Levitus, S., 1994. World Ocean Atlas 1994, National Oceanographic Data Center, http://www.cdc.neaa.gov/cdc/data.nodc.woa94.html.

Madsen, O.S., 1977. A realistic model of the wind-induced Ekman boundary layer. Journal of Physical Oceanography 7, 248–255.

Montecinos, A., 1991. El efecto del fenómeno de El Niño en los vientos favorables a la surgencia costera. Oceanographer Thesis, Universidad Católica de Valparaíso, Chile

Pares-Sierra, A., O'Brien, J.J., 1989. The seasonal and interannual variability of the California Current System: A numerical model. Journal of Geophysical Research 94, 3159–3180.

Pizarro, O., 1999. Low frequency fluctuations in the Eastern Bounday Current off South America: Remote and local forcing. ISSN 140-3813. Distribution: Earth Sciences Centre, Göteborg, Sweden.

Pizarro, O., Hormazábal, S., González, A., Yánez, E., 1994. Variabilidad del viento, nivel del mar y temperatura en la costa norte de Chile. Investigaciones Marinas, Valparaíso 22, 85–101.

Richards, F.A. (Ed.), 1981, Coastal Upwelling. American Geophysical Union, Washington, DC.

Rojas de Mendiola, B., 1981. Seasonal phytoplankton distributions along the Peruvian coast. In: Richards, F.A. (Ed.), Coastal Upwelling. American Geophysical Union, Washington DC, pp. 348–356.

Ruggles, K.W., 1970. The vertical mean wind profile over the ocean in light to moderate winds. Jr. Application Meleorology 9, 389–395.

Schwerdtfeger, W., 1976. Climates of central and South America. In: Schwerdtfeger, W. (Ed.), World Survey of Climatology, vol. 12. Elsevier, Amsterdam.

Shaffer, G., Pizarro, O., Djurfeldt, L., Salinas, S., Rutllant, J., 1997. Circulation and low frequency variability near the Chile coast: remotely forced fluctuations during the 1991-1992 El Niño. Journal of Physical Oceanographys 27, 217–235.

Shaffer, G., Hormazabal, S., Pizarro, O., Salinas, S., 1999. Seasonal and interannual variability of currents and temperature over the slope of central Chile. Journal of Geophysical Research 104 (C12), 29951–29961.

Soto-Mardones, L., Pares-Sierra, A., Salinas, S., 2004. Annual and interannual variability of the SST (AVHRR-Hydrographic) off Chile (18°–40°S). Journal of Geophysical Research, submitted for publication.

Strub, T.P., Mesias, J., Montecino, V., Rutllant, J., Salinas, S., 1998. Coastal ocean circulation off western South America. The Sea 11, 273–313.

Weare, B. C., Strub, P. T., Samuel, M. D., 1980. Marines climates atlas of the tropical Pacific Ocean Contribution in Atmospheric Sciences, vol: 20. University of California, Davis, 147pp.